PHYSICAL REVIEW B VOLUME 36, NUMBER 11 15 OCTOBER 1987-I

Monte Carlo investigation of the electron-hole-interaction effects on the ultrafast relaxation of hot photoexcited carriers in GaAs

M. A. Osman* and D. K. Ferry
Center for Solid State Electronics Research, Arizona State University, Tempe, Arizona 85287-6206
(Received 24 April 1987)

The roles of the electron-hole (*e-h*), electron-electron (*e-e*), hole-hole (*h-h*), and screened electron-phonon (*e*-ph) interactions on the ultrafast relaxation of photoexcited carriers in GaAs are examined. Theoretical expressions for the various scattering rates are obtained, and these are used in an ensemble Monte Carlo calculation. At low carrier concentrations the *e*-ph interaction is the main energy-loss channel for hot electrons, while at high carrier concentrations the *e-h* interaction is the primary energy-loss channel. This latter result follows from the high *e-h* scattering rate, the screening of the *e*-ph interaction, and the high efficiency of hole-phonon scattering through the unscreened deformation-potential interaction. The electron energy-loss rates through the *e-h* interaction increase as the excitation energies and intensities are increased. For excitation by an excess photon energy of 130 meV, for example, it is found that the *e-e* interaction slows the cooling rates at all excitation levels, while the *h-h* interaction enhances the cooling rate of the holes.

I. INTRODUCTION

Progress in the generation of ultrashort pulses and their application in studying the phenomena on a picosecond time scale has made it possible to investigate processes such as cooling rates of photoexcited carriers,[1-2] the lifetimes of phonons,[3] the screening of optical-phonon–carrier interactions,[4] and velocity overshoot in semiconductors,[5] which all occur on the subpicosecond time scale. Several models have been developed to explain the role of processes such as screening of LO-phonon–carrier interactions,[6] hot phonons,[7,8] and electron-hole (*e-h*) interaction[9] in the observed cooling rates of the excited carriers. Although carriers are generated monoenergetically, and the time scales involved are very short for a standard distribution to be defined, most previous models assumed either Fermi-Dirac or Maxwell-Boltzmann statistics. Furthermore, the electrons and holes were assumed to have equal temperatures even though initially the energies of the electrons and holes are quite different. Even when different temperatures for electrons and holes[9] were assumed, the form of the distribution function was imposed in order to study transients on the subpicosecond time scale. However, these approaches are valid only on time scales that are large compared with the relaxation time for information on a microscopic scale, which is the time for the system to lose the memory of the initial distribution[8] and to reach a quasiequilibrium state. This inherently assumes that the system has thermalized through the carrier-carrier interaction processes, at which point the form for the nonequilibrium distribution function can be defined. Additionally, the presence of the higher valleys in GaAs is usually neglected, even at excess energies ranging from 0.5 to 2.5 eV, in order to avoid the complications of the resulting coupled system of transport equations.

Because the initial rapid thermalization of the photoexcited electron-hole plasma occurs though carrier-carrier interactions, the understanding of the cooling process requires a knowledge of how this thermalization proceeds on the subpicosecond time scale. More specifically, the manner in which the *e-e*, *h-h*, and *e-h* interactions influence the cooling of the photoexcited carriers at different excitation energies and levels is required to understand the dynamics of carriers on a subpicosecond time scale. The *e-e* (and *h-h*) scattering process is quasielastic, in that the energy of the electron (hole) system is conserved. This has led some researchers to consider that the *e-h* scattering was elastic, so that the energy of the electron in the initial and final states was the same.[10] This is justified only if the mass of the hole is infinitely larger than that of the electron. Takenaka,[11] using a Monte Carlo technique, has also assumed that the electron-hole interaction is similar to the ionized impurity scattering, so that no energy exchange is involved in this process.

On the other hand, the recent experiments using picosecond and subpicosecond laser pulses have revealed new information about the nature of the electron-hole interaction and how it influences the transport properties of semiconductors. Höpfel *et al.*[2,12] have observed that the energy-loss rates for the photoexcited electrons were doubled in the presence of a cold hole plasma, and that minority electrons in quantum-well structures exhibit absolute negative mobility at low temperatures and low electric fields. Similarly, Degani *et al.*[13] have observed an increase in the saturation velocity of the minority photoexcited electrons in *p*-type $Ga_{0.53}In_{0.47}As$ and no negative-differential-resistance effect for the minority electrons. Instead, the velocity continued to increase throughout the range of electric fields used in their experiment. All of the above observations have been attributed to the energy exchange between the minority

electrons and holes which tends to transfer the energy from the hot electrons to the holes. Consequently, the above models for the electron-hole interaction do not explain these observed phenomena and there is a need to treat the electron-hole interaction without making any *a priori* assumptions about the magnitudes of the energy involved in the scattering process.

In this paper, the role of the *e-h* interaction in the ultrafast relaxation of hot photoexcited carriers is examined at different excitation levels and energies using the ensemble Monte Carlo approach. The details of the model used in the simulation are discussed in the next section. The theory of the *e-h* and screened electron-phonon (*e*-ph) interactions is developed in Sec. III and the expressions for the scattering rates of the *e-e*, *e-h*, *h-h*, and screened *e*-ph and *h*-ph interactions are also derived. Similarly, the self-consistent screening model is discussed and the expression for the screening length is given. The results of the simulation are discussed in Sec. IV, with special emphasis on the role of the *e-h* interaction in the relaxation of the photoexcited electrons and holes. In addition, the influence of the screening and the manner in which the *e-e* (*h-h*) interaction affects the relaxation of the electrons (holes) are examined. Furthermore, the energy-loss rates of electrons through the *e-h* and *e*-ph interactions are studied as a function of excitation energy and level. The time evolution of the energy distribution function of electrons for various combinations of scattering processes is also obtained. Finally, the summary and conclusions are given in Sec. V.

II. THE APPROACH

The dynamics of electrons and holes was studied using the ensemble Monte Carlo (EMC) approach, which has been shown to be suitable for studying the fast transients.[14] The model takes into account the *e-e*, *e-h*, *h-h*, carrier-phonon, and carrier-impurity scattering. Furthermore, the screening of the *e*-ph and *h*-ph interactions in polar semiconductors is included self-consistently in the static and long-wavelength limit of the random-phase approximation. The conduction-band model consists of three nonparabolic valleys, while the valence band consists of a parabolic heavy-hole band (the light hole is included in the model but ignored in this investigation). The inter–valence-band hole-hole and screened light-hole–phonon scattering are built into the model, but as mentioned, the role of the light holes has been ignored in the present calculation because of their small population (less than 10% of the holes) and also to reduce the required computational time by eliminating the need to self-consistently calculate the scattering rates for the light-hole processes. However, the strong coupling between the heavy and light holes through the *h-h* interaction, combined with the expected high efficiency of the interactions between the light holes and the electrons in exchanging momentum and energy, might lead to enhancement of the electron energy-loss rates through the electron–light-hole interaction. The investigation of the role played by the light holes is currently underway and will be published elsewhere.

The present analysis deals mainly with a lattice temperature of 77 K and excess electron energies below the energy difference of the L valleys (from the zone-center Γ valley). Under these conditions, the acoustic phonon scattering is elastic and the interaction between the electrons, which may reside in the L valleys, and the holes is negligible. The elastic impurity scattering is ignored in our calculation, since we assume that all of the carriers are generated by the photoexcitation process. In order to examine the role of the *e-h* interaction more closely, the phonon system was assumed to be in equilibrium. This is a significant assumption, but our purpose here is to examine the role of the *e-h* interactions. Subsequent work will address the interplay between this process and the nonequilibrium phonons.

Because the initial energy of the electron is about seven times larger than the hole's energy (for 130 meV

TABLE I. Parameters for GaAs electron transport program.

Parameter		Value		
		Γ valley	L valley	X valley
Density (g/cm^3)	5.37			
Energy-band gap at 77 K (eV)	1.51			
High-frequency dielectric constant	10.92			
Static dielectric constant	12.9			
Lattice constant (cm)	5.65×10^{-8}			
Number of valleys		1	4	3
Effective mass ratio		0.063	0.222	0.58
Nonparabolicity factor (eV^{-1})	(300 K)	0.61	0.46	0.20
	(77 K)	0.58	0.44	0.19
Valley separation from Γ valley (eV)			0.29	0.522
Polar optic-phonon energy (eV)		0.036	0.036	0.036
Acoustic deformation potential (eV)		7.0	7.0	7.0

TABLE II. Parameters for GaAs hole-transport program.

	Bulk material parameters	
Crystal elastic constants (dyn/cm^2):	C_{11}	11.88×10^{11}
	C_{12}	5.38×10^{11}
	C_{44}	5.49×10^{11}
[100] longitudinal sound velocity S_l (cm/sec)		4.73×10^{5}
[100] transverse sound velocity S_t (cm/sec)		3.34×10^{5}
	Scattering-rate parameters	
Effective masses:	heavy-hole band m_{HH}	$0.45m_0$
	light-hole band m_{LH}	$0.082m_0$
Optical-phonon energy (eV)		0.036
Deformation-potential constants (eV):	a	6.7
	b	1.7
	d	4.4

excess energy, the electron gains 113 meV), the electron-hole plasma forms a thermodynamically far-from-equilibrium system. Consequently, one expects that energy will be transferred from the hot electrons to the cold holes and to the lattice through the electron-hole interaction and the electron-phonon interaction, respectively. To achieve this, a good model of the material must be achieved. The parameters for the electron and hole transport are shown in Tables I and II, respectively. The values for the equivalent and nonequivalent intervalley phonon energies and deformation potentials, which give a good fit for the velocity-field characteristics for electrons in GaAs,[15] are given in Table III. The hole transport parameters are essentially the same as those used by Brennan and Hess,[16] except for the deformation-potential constant b, which was reported by Madelung.[17] These constants give a good fit for the experimental velocity-field measurements and result in a stronger role played by the deformation-potential interaction, which has been observed in p-type III-V compounds.[18,19] Figure 1 is a flow chart of the EMC program used in this investigation. The first step corresponds to specifying the material parameters, initial energy distribution of the carriers, pulse shape and duration, lattice temperature, value of the electric field, and which carrier-carrier (c-c) interactions are active. The scattering rates for the acoustic phonons, deformation-potential optical phonons, and intervalley phonons are then calculated and tabulated. On the other hand, the scattering rates of the various c-c and screened carrier-phonon interactions, which depend upon the evolving distribution function of the carriers, are calculated every 50 fs initially, and at longer intervals as the time proceeds and changes occur more slowly. For finite pulse duration, the number of carriers is adjusted according to the pulse shape, with an initial energy determined from the energy of the pulse, taking into account the nonparabolicity of the conduction (or valence) band. The dynamics of the electrons and holes is then examined using the regular EMC approach. Coupling between the electron EMC and the hole EMC programs is accomplished through the e-h interaction, which depends on the energy and momentum distribution of the

TABLE III. Intervalley coupling constants and phonon energies.

Transition	Coupling constant (10^8 eV/cm)	Phonon energy (eV)
Γ-L	10	0.0278
Γ-X	7	0.0299
L-L	10	0.0278
L-X	5	0.0293
X-X	7	0.0299

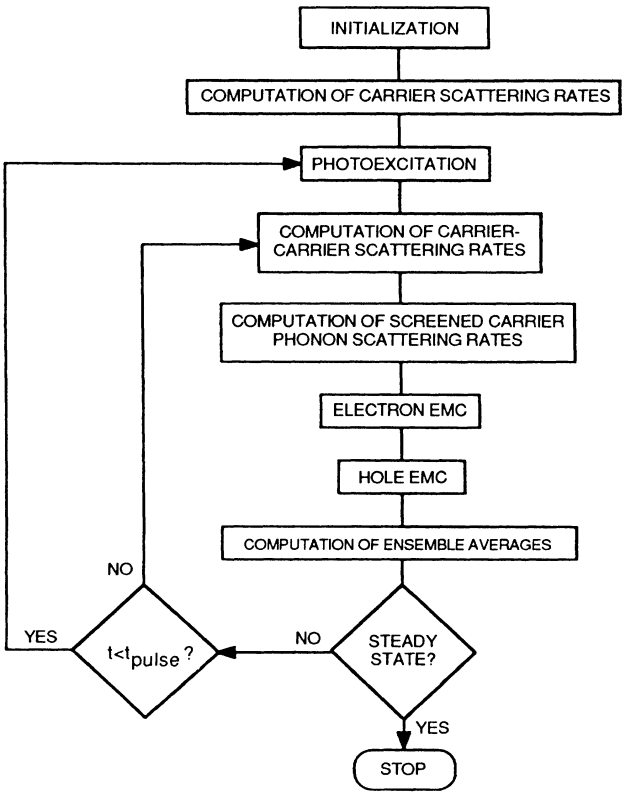

FIG. 1. Flow chart of the ensemble Monte Carlo (EMC) program.

electrons and holes. The average energy of the electrons and holes, energy-loss rates through *e-h* and *e*-ph interactions, are then calculated at the end of each iteration or at specified time intervals.

III. THEORY

The carrier-carrier interaction is very important at high carrier densities. Furthermore, each carrier, while interacting with the phonons, is influenced by the presence of the other carriers. Consequently, the carrier-carrier interactions screen the carrier-phonon interactions. This screening considerably weakens the electron-phonon interactions compared to the hole-phonon interactions. This is because holes also interact with TO phonons through the practically unscreened deformation-potential coupling.[7] The *e*-ph interaction is strongly screened at high concentrations of electrons where the Puali exclusion principle has to be taken into account. This makes the *e*-ph interactions very inefficient as a channel for transferring the excess energy of the hot electrons to the lattice. On the other hand, the *h*-ph interactions are very efficient in transferring the energy from the hot holes to the lattice. Furthermore, the photoexcitation process generates electrons with excess energy much higher than that of holes, on account of the band structure. This results in a two-carrier system that is very far from equilibrium. The optimum manner in which the system can reach equilibrium is by transferring energy from the hot electrons to the relatively cold holes and then to the lattice. The effects of exchange forces, band-gap renormalization, and state filling[20] are neglected. In addition, we also neglect the mixing of the longitudinal-optical phonons and the plasmon modes.[21] In Sec. III A, the scattering reates for carrier-carrier interactions are derived. The screened *e*-ph and *h*-ph interactions are then derived in Sec. III B, and the self-consistent screening model is discussed briefly. The expressions for the energies of the photoexcited *e-h* pairs are developed in Sec. III C.

A. Screened carrier-carrier interaction

The electron and holes are assumed to interact among themselves, and with each other, through a screened Coulomb potential of the form

$$V(r)=\frac{e^2}{4\pi\epsilon r}\exp(-\beta r)\ , \tag{1}$$

where ϵ is the dielectric constant of the material and β is the inverse screening length. The probability for the two interacting fermions to make a transition from the initial state $(\mathbf{k}_0,\mathbf{k})$ to a final $(\mathbf{k}_0',\mathbf{k}')$ as a result of the Coulomb interaction is obtained from the Fermi golden rule as

$$S_{k_0,k\to k_0',k'}=\frac{2\pi}{\hbar}|M|^2 f_{k_0}f_k(1-f_{k_0'})(1-f_{k'}) \times\delta(E_{k_0'}+E_{k'}-E_{k_0}-E_k)\ , \tag{2}$$

where f_k and E_k are the occupation probability and the energy of the wave vector $\mathbf{k}$, respectively, and similarly for the other wave vectors. The matrix element M is given by

$$M=\langle\mathbf{k}_0,\mathbf{k}\,|\,V(r)\,|\,\mathbf{k}_0',\mathbf{k}'\rangle=\frac{e^2}{V\epsilon}\frac{\delta_{\mathbf{k}_0+\mathbf{k},\mathbf{k}_0'+\mathbf{k}'}}{|\mathbf{k}_0'-\mathbf{k}_0|^2+\beta^2}\ , \tag{3}$$

where V is the volume of the crystal, and the initial and final states have been represented by plane waves. The scattering rate for the carrier-carrier interaction is obtained from (2) by summing over $\mathbf{k}$, $\mathbf{k}'$, and $\mathbf{k}_0'$. Because the manner in which degeneracy is implemented in EMC decides whether the final state is occupied or not after selecting the scattering mechanism, all the final states are assumed to be unoccupied in the calculation of scattering rates.[22] Consequently, we can assume that all the final states are empty, i.e., $f_{k_0'}=f_{k'}=0$ (furthermore, we set $f_{k_0}=1$). Under these conditions the scattering rate for an electron in state $|\mathbf{k}_0|\rangle$ by a hole in state $|\mathbf{k}\rangle$, assuming parabolic energy momentum dispersion $(E=\hbar^2k^2/2m^*)$ for both the electrons and holes, is given by

$$\Gamma_{eh}(\mathbf{k}_0)=\frac{\mu e^4}{2\pi\hbar^3\epsilon^2V}\sum_{\mathbf{k}}f_k\,\mathbf{g}/(g^2+\beta^2)\ , \tag{4}$$

where the relative wave vector $\mathbf{g}$ and reduced mass μ are defined by

$$\mathbf{g}=2\mu(\mathbf{k}_0/m_e-\mathbf{k}/m_h)$$

and

$$\mu=m_em_h/(m_e+m_h)\ . \tag{5}$$

We can gain more insight into this process by rewriting (4) in integral form for both $\Gamma_{eh}(\mathbf{k}_0)$ and $\Gamma_{he}(\mathbf{k}_0)$, i.e.,

$$\Gamma_{eh}(\mathbf{k}_0)=\frac{p\mu e^4}{2\pi\epsilon^2\hbar^3}\int d^3k\,f_h(k)\frac{Q_{eh}}{\beta^2(Q_{eh}^2+\beta^2)} \tag{6}$$

and

$$\Gamma_{he}(\mathbf{k}_0)=\frac{n\mu e^4}{2\pi\epsilon^2\hbar^3}\int d^3k\,f_e(k)\frac{Q_{he}}{\beta^2(Q_{he}^2+\beta^2)}\ , \tag{7}$$

where

$$Q_{eh}=2\mu|\mathbf{k}_0/m_e-\mathbf{k}/m_h|\ ,\quad Q_{he}=2\mu|\mathbf{k}_0/m_h-\mathbf{k}/m_e|\ , \tag{8}$$

and n and p are the electron and hole concentrations. It is obvious that in general $\Gamma_{eh}\neq\Gamma_{he}$, because of the large density of states in the heavy-hole band compared to the central valley of the conduction band. Moreover, the two distribution functions can be dramatically different in detail. This situation arises particularly in the photoexcitation of *e-h* plasmas, because the initial energy of the electrons is usually much higher than that of the holes. Furthermore, the concentrations of electrons can be different from that of the holes in the situation in which the starting semiconductor material is doped significantly.

Expressions (6) and (7) are not suitable for calculating the scattering rates in the ensemble Monte Carlo method

because one has to know the form of the electron and hole distribution functions. Takenake *et al.*[11] assumed $f_e(k)$ to be a drifted Maxwellian in order to evaluate the *e-e* scattering rate numerically. Although this assumption is justified for steady-state situations, it does not hold in transient situations following the application of a laser pulse or electric field. Lugli and Ferry[23] used the time-evolving distribution function built into the EMC approach to calculate the *e-e* scattering rates self-consistently. Their algorithm eliminated the need to know the form of the distribution function and allowed them to study the effect of *e-e* interactions in transient situations. The basic idea behind their approach is the realization of the fact that the ensemble average $\langle G(k)\rangle$ of any k-dependent microscopic observable $G_i(k)$ of the ith particle of the ensemble is given by

$$\langle G(k)\rangle = \int d^3k\, G(k) f(k) = \frac{1}{N}\sum_{i=1}^{N} G_i(k)\ , \tag{9}$$

where N is the number of carriers in the ensemble. In a similar fashion, using the fact that the integral over the distribution function is equivalent to a sum over all the ensemble, the expressions for the scattering rates can be rewritten as

$$\Gamma_{eh}(\mathbf{k}_0) = \frac{p\mu e^4}{2\pi\epsilon^2\hbar^3}\frac{1}{N_h}\sum_{\text{holes}}\frac{Q_{eh}}{\beta^2(Q_{eh}^2+\beta^2)} \tag{10}$$

and

$$\Gamma_{eh}(\mathbf{k}_0) = \frac{n\mu e^4}{2\pi\epsilon^2\hbar^3}\frac{1}{N_e}\sum_{\text{electrons}}\frac{Q_{he}}{\beta^2(Q_{he}^2+\beta^2)}\ . \tag{11}$$

To obtain the expression for the *e-e* scattering rate $\Gamma_{ee}(\mathbf{k}_0)$, we set $m_e = m = m_h$ and $\mu = m/2$ in (10) (choosing the appropriate mass for the electrons and conversely for the holes in *h-h* scattering), and

$$\Gamma_{ee}(\mathbf{k}_0) = \frac{nme^4}{4\pi\epsilon^2\hbar^3}\frac{1}{N_e}\sum_{\mathbf{k}}\frac{|\mathbf{k}_0-\mathbf{k}|}{\beta^2(|\mathbf{k}_0-\mathbf{k}|^2+\beta^2)}\ , \tag{12}$$

where N_e (N_h) are the number of electrons (holes) in the ensemble and the sum is over all the $\mathbf{k}$ vectors of the ensemble carriers. The major advantage of the above expressions for the scattering rates is the elimination of the need to explicitly know the form of the distribution function. Furthermore, because the EMC has a built-in distribution function, these expressions make use of the actual distribution function as it evolves in time with the ensemble. Consequently, one can study the relaxation of highly excited carriers, taking into account the carrier-carrier interaction on a subpicosecond time scale.

The magnitude of the relative wave vector $\mathbf{g}$ is conserved in the collision, which allows one to determine the relative wave vector $\mathbf{g}'$, and hence $\mathbf{k}_0'$ and $\mathbf{k}'$, from the following relations:

$$\mathbf{k}_0' = \mathbf{k}_0 - \tfrac{1}{2}(\mathbf{g}'-\mathbf{g})\ ,$$
$$\mathbf{k}' = \mathbf{k} + \tfrac{1}{2}(\mathbf{g}'-\mathbf{g})\ . \tag{13}$$

The final states are then checked to see if they are allowed, to account for degeneracy in a manner similar to that described by Lugli and Ferry.[22] If either $\mathbf{k}'$ or $\mathbf{k}_0'$ is not allowed, the scattering event is taken as a self-scattering, i.e., the states of two particles are not changed.

The above scattering rates describe the scattering of the primary particle. We have chosen to change the state of the second particle taking part in the carrier-carrier interaction to conserve both the energy and momentum, even though this means some of the carriers will scatter more frequently.

In Fig. 2, we plot the scattering rates for *e-e*, *e-h*, and *h-h* interaction processes, assuming a Maxwellian distribution for both the electrons and holes, for illustrative purposes. In this way, we have assumed the electron temperature is 1100 K and the hole temperature is 160 K. From this figure, it is clear that the *h-h* scattering rates are much stronger than the *e-e* scattering rates due to the larger density of states in the heavy-hole band. Also notice that the interaction of an electron with a hole plasma is stronger than the rate at which a hole interacts with a sea of electrons. This is related to the large density of states for holes also.

B. Screened carrier-phonon interactions

The electron-electron interaction modifies the electron-phonon interaction by screening these interactions. Assuming static screening, the expression for the screened electron-phonon interaction is

$$V_{\text{ph}}^{s}(q) = \frac{e^2\hbar\omega_0}{\epsilon V}\left[\frac{1}{\epsilon_\infty}-\frac{1}{\epsilon_0}\right]\frac{q^2}{(q^2+\beta^2)^2}\ , \tag{14}$$

where β is the inverse screening length. The total scattering rate is given by

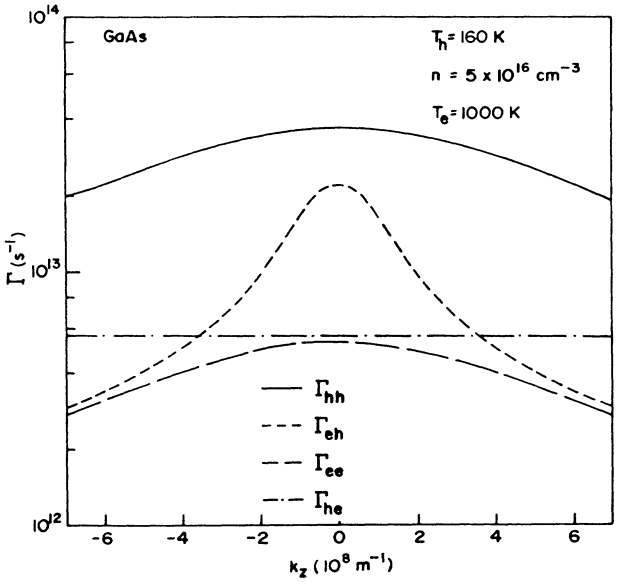

FIG. 2. Carrier-carrier scattering rates as a function of the average z-directed momentum.

$$\Gamma^s_{p0}(E)=A\frac{\gamma(E')}{\gamma^{1/2}(E)}\left[\ln\left[\frac{u}{z}\right]-E_\beta\left[\frac{1}{z}-\frac{1}{u}\right]\right]$$
$$\times(N_0+\tfrac{1}{2}\pm\tfrac{1}{2}) , \quad (15)$$

where

$$A=(2m)^{1/2}\frac{e^2\hbar\omega_0}{16\pi\epsilon\hbar^2}\left[\frac{1}{\epsilon_\infty}-\frac{1}{\epsilon_0}\right] ,$$
$$u=[\gamma^{1/2}(E)+\gamma^{1/2}(E')]^2+E_\beta ,$$
$$z=[\gamma^{1/2}(E)-\gamma^{1/2}(E')]^2+E_\beta ,$$
$$E_\beta=\frac{\hbar^2\beta^2}{2m} ,$$
$$E'=E\mp\hbar\omega_0 .$$

The angular dependence of the scattering is determined from

$$P(k,\cos\theta)=\frac{[(k')^2+k^2-2kk'\cos\theta]}{[(k')^2+k^2-2kk'\cos\theta+\beta^2]^2} , \quad (16)$$

using the rejection method.[24]

Similarly, the total screening rate for intraband scattering of the screened heavy-hole–phonon interaction is given by

$$\Gamma^s_{11}(E)=A\Psi(E)G_{11}(E)E^{-1/2}(N_0+\tfrac{1}{2}\pm\tfrac{1}{2}) , \quad (17)$$

where A has the same meaning as above except for the obvious change in carrier mass, and

$$\Psi(E)=\ln\left[\frac{[E^{1/2}+(E')^{1/2}]^2+E_\beta}{[E^{1/2}-(E')^{1/2}]^2+E_\beta}\right] ,$$

E_β has the obvious change of carrier mass,

$$G_{11}=\tfrac{1}{4}\left\{1+3\Phi\left[\Phi-\frac{2}{\Psi}\right]+6(\Phi-\xi)\left[\Phi-\left[1+\frac{\Phi^2}{\Phi^2-1}\right]\Psi^{-1}\right]\right\} ,$$
$$\Phi(E)=\frac{E+E'+E_\beta}{2(EE')^{1/2}} ,$$
$$\xi(E)=(E+E')/2(EE')^{1/2} .$$

The scattering rates for the light holes are obtained by replacing the heavy-holes mass m_1 by the light-hole mass m_2 in the above expressions. For interband transitions from the heavy-hole band to the light-hole band, the total scattering rate is

$$\Gamma^s_{12}(E)=A_{12}\Psi_{12}(E)G_{12}(E)E^{-1/2}(N_0+\tfrac{1}{2}\pm\tfrac{1}{2}) . \quad (18)$$

Here,

$$A_{12}=\frac{e^2\hbar\omega_0}{16\pi\epsilon\hbar^2}m_2(2/m_1)^{1/2}\left[\frac{1}{\epsilon_\infty}-\frac{1}{\epsilon_0}\right] ,$$
$$\Psi_{12}(E)=\ln\left[\frac{[E^{1/2}+(m_2E'/m_1)^{1/2}]^2+E_\beta}{[E^{1/2}-(m_2E'/m_1)^{1/2}]^2+E_\beta}\right] ,$$
$$G_{12}(E)=\tfrac{3}{4}[1-\Phi_{12}(\Phi_{12}-2\Psi_{12}^{-1})-2(\Phi_{12}-\phi_{12})(\Phi_{12}-2\Psi_{12}^{-1})] ,$$

and

$$\Phi_{12}=\frac{E+(m_2/m_2)E'_2+E_\beta}{2[E(m_2/m_1)E']^{1/2}} ,$$
$$\phi_{12}=\frac{E+(m_2/m_1)E'}{2[m_2/m_1)E'E]^{1/2}} .$$

By interchanging the subscripts 1 and 2 in the above expressions we get the total scattering rate for light-hole to heavy-hole band transitions.

The angular dependence of the scattering is determined from the following expressions:

$$P_{11}(k_1\cos\theta)\sim\frac{[k^2+(k')^2-2kk'\cos\theta](1+3\cos^2\theta)}{[k^2+(k')^2-2kk'\cos\theta+\beta^2]^2} , \quad (19)$$

and

$$P_{12}(k_1\cos\theta)\sim\frac{[k^2+(k')^2-2kk'\cos\theta](1-\cos^2\theta)}{[k^2=(k')^2-2kk'\cos\theta+\beta^2]^2} , \quad (20)$$

for the intraband and interband transitions, respectively.

The energy dependence of the scattering rate for electron temperature $T_e=1000$ K at $T=77$ K is shown in Fig. 3 for concentration levels of 5×10^{17} and 10^{18} cm^{-3}. In Fig. 4, the scattering rates in the presence of holes at

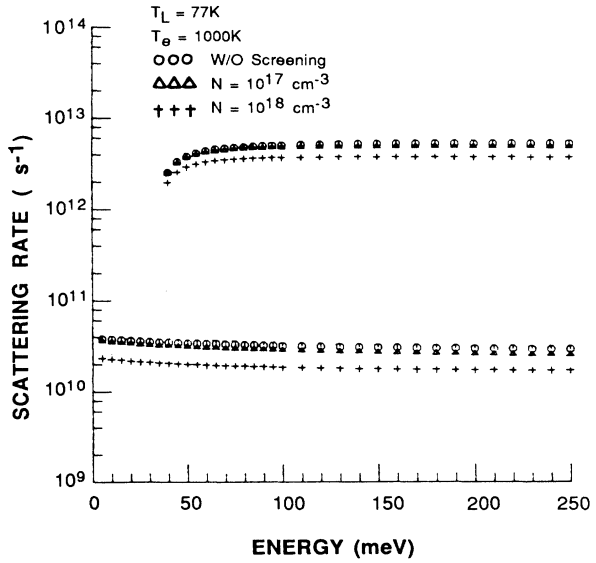

FIG. 3. Energy dependence of the screened electron-phonon scattering rates in GaAs for various electron concentrations, neglecting the presence of the holes, at 77 K.

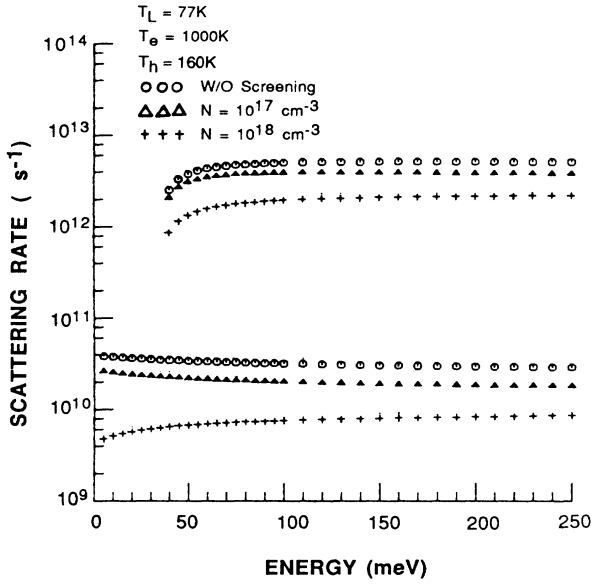

FIG. 4. Energy dependence of the screened electron-phonon scattering rates in GaAs in the presence of equal concentrations of electrons and holes, for various electron concentrations, at 77 K.

$T_h = 160$ K and a concentration similar to that occurring in photoexcitation are shown. From these plots, it is obvious that screening is effective at high carrier concentrations and low temperatures. This reduction in the scattering rates at high concentration will slow down the cooling rate of the hot photoexcited carriers. The presence of the electrons does not influence the screening in the same way as holes affect the scattering rates for electrons. This is because the holes have lower average energy so that the screening length is more or less determined by the hole themselves.

The Debye-Hückel screening model was used to calculate β in the plotted scattering rates, which is given by

$$\beta^2 = \frac{ne^2}{\epsilon k_B T_e} , \tag{21}$$

and in the presence of holes at temperature T_h by (for the assumption of equal concentrations of electrons and holes used in this study)

$$\beta^2 = \frac{ne^2}{\epsilon k_B}\left[\frac{1}{T_e}+\frac{1}{T_h}\right] . \tag{22}$$

However, in this investigation the screening length was calculated self-consistently, which is different from all previous EMC investigations of carrier-carrier interaction effects[11,23] which have used the Debye-Hückel screening model. Although this is a consequence of assuming a Maxwell-Boltzmann distribution of the carriers, it is justified under steady-state conditions but is not valid for systems that are far from equilibrium. Thus, to study the fast transients properly using EMC, one has to calculate the screening length self-consistently using the evolving built-in distribution function. In the static and long-wavelength limit of the random-phase approximation, β^2 is proportional to the ensemble average of $B(E)$ and is given by

$$\beta^2 = \frac{ne^2}{\epsilon_s}\frac{1}{N}\sum_{i=1}^{N} B(E_i) , \tag{23}$$

where N is the number of carriers in the ensemble. The form of $B(E)$ depends on the band model used in EMC calculation and is given by

$$B(E) = 1/2E ,$$

and

$$B(E) = \frac{2\alpha}{1+2\alpha E} + \frac{1+2\alpha E}{2E(1+\alpha E)} , \tag{24}$$

for parabolic and nonparabolic bands, respectively.

C. The excess energies of photoexcited electron-hole pairs

The excess energy of the electron-hole pairs excited by a photon of energy $\hbar\omega$ is evaluated using the band model discussed in Sec. II. The excess energy ΔE_h of the hole is given by

$$\Delta E_h = (1/2\alpha)\Gamma(1-\{1-4\alpha(\hbar\omega-E_g) \times[1+\alpha(\hbar\omega-E_g)]\}^{1/2}/\Gamma) \tag{25}$$

and

$$\Delta E_e = (\hbar\omega-E_g)-\Delta E_h ,$$

respectively, where

$$\Gamma = 1+m_h/m_e+2\alpha(\hbar\omega-E_g) ,$$

m_e (m_h) is the electron (hole) mass, E_g is the energy gap, and α is the nonparabolicity factor. We have neglected the inhomogeneity in the spatial carrier distribution. This amounts either to assuming that the excitation of carriers is achieved via a two-photon absorption process or by considering the transport in a very thin layer near the surface of the material, which in either case means that the sample thickness is small compared to the absorption depth. The generation of carriers was achieved either by simulating a laser pulse of subpicosecond duration, or by starting from an initially monoenergetic distribution of carriers. The latter amounts to assuming that the pulse is a delta function in time, which is ideal for examining the cooling process, since the complications due to the continuous generation of carriers is avoided.

IV. RESULTS

The cooling of the photoexcited carriers was investigated for different excitation levels, ranging from 5×10^{16} to 1×10^{18} cm^{-3}, at three different photon energies (1.55, 1.64, and 1.71 eV) which correspond to excess energies of 40, 130, and 200 meV, respectively. The pulse duration was taken to be either 0.2 ps or a delta

function in time. In the following sections, the manner in which the screening of the carrier-phonon interactions and the *e-h*, *e-e*, and *h-h* interactions influence the cooling process are discussed.

A. Effect of carrier-phonon screening

The cooling rates of the photoexcited electrons were examined in the absence of the *c-c* interactions, using both the Debye-Hückel and the self-consistent screening models. This was done to compare the results of the simulation to previous models which either assumed equal electron and hole temperatures or totally ignored the presence of holes on account of the small fraction of energy they receive in the photoexcitation process. In Fig. 5, we illustrate the results. Curve 1 corresponds to the situation where the screening is totally ignored, which predicts a very fast cooling rate in contrast to the observed slow cooling rates at high excitation levels. When the screening of the *e*-ph interaction is taken into account, while the presence of the photoexcited holes is ignored, the cooling rate is slightly reduced, as shown by curve 2. However, when the presence of the photoexcited holes is included, using the same screening model, the cooling rate is significantly decreased, which is shown by curve 3.

Immediately after excitation, the distribution function is significantly different from the Maxwellian upon which the Debye-Hükel model is based. We have examined the importance of the distribution in screening by using the self-consistent screening model discussed above. The cooling rates shown by curves 4 and 5 in Fig. 5 correspond to situations where the presence of the holes is either ignored (curve 4) or included (curve 5). From these cooling rates, it is obvious that the screening length for the *e-h* plasma is controlled by the holes which are initially generated at lower energies, and also thermalize at a faster rate due to the strength of the *h-h* interaction. This is obvious from the expression for the screening length given above, which shows that the screening length is inversely proportional to the carrier temperature. Furthermore, the fact that the decrease in the cooling rate is smaller for the self-consistent screening model reflects the evolution of the distribution function of the carriers. On the other hand, the Debye-Hückel model assumes an equilibrium distribution, so that the screening is dominated by the cold (low-energy) carriers, which do not exist in the first stages of the cooling of photoexcited plasmas.

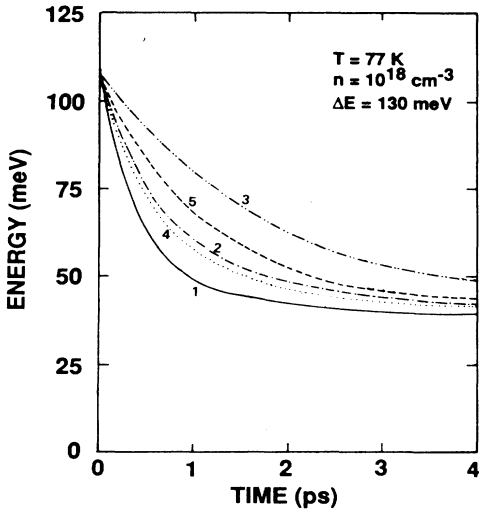

FIG. 5. Time dependence of the mean energy of electrons for different screening models of the electron-phonon interactions: curve 1, no screening; curve 2, Debye screening by only the electrons; curve 3, Debye screening by both the electrons and the holes; curve 4, self-consistent screening by only the electrons; and curve 5, self-consistent screening by both the electrons and the holes.

B. The effect of electron-hole interaction

The investigation of the cooling rates in the previous section assumed that the electrons and holes cool independently. Thus there was no coupling between the cooling rates of the electrons and the holes, and no energy transfer from one system component to the other. Because the initial energy of the electron is about seven times that of the hole, the *e-h* plasma forms a far-from-equilibrium plasma in which one component is significantly hotter than the other. Consequently, one expects energy transfer from the hot electron system to the relatively cold hole system and the role of *e*-ph and *h*-ph interactions to vary accordingly. The relative importance of the *e-h* and *e*-ph interactions as energy-transfer channels depends upon the excitation level and energy. The details of these cooling processes were investigated over the range of densities mentioned above, but only at the single laser energy of 1.64 eV.

First, the simulation was carried out assuming only phonon interactions were active. Curve 1 in Figs. 6 and 7 corresponds to this situation and it is obvious from comparing Figs. 6(a) and 6(b) that the electrons cool faster at low photoexcited-carrier concentrations where the screening is negligible. On the other hand, curve 1 in Fig. 7, which represents the cooling of holes, does not vary with time, since the holes are generated with energies below the phonon emission threshold, which together with the fact that at 77 K the phonon absorption process is negligible, puts a severe restriction on the role the optical phonons can play in the cooling process.

In the second step, the electron-electron and hole-hole interactions were included in addition to the optical-phonon interaction. Curve 2 in these figures shows the cooling process for the electrons and holes. The most interesting phenomenon is that the *h-h* interaction enhances the cooling of the hole system, while the *e-e* interaction slows the cooling process of the electrons. The enhancement in the cooling of the hole system can be attributed to the fact that the *h-h* interaction is very strong, and the fact that the energy exchange between the holes increases the energy of some holes above the phonon emission threshold, so these can then emit phonons through the optical deformation-potential interac-

tion. On the other hand, the interaction among the electrons quickly redistributes the electrons into high- and low-energy regions, as we will show in the discussion of the evolution of the distribution function. Thus, many electrons end up in regions where they cannot emit optical phonons, while those which end up in the higher-energy regions essentially have the same probability for emission of optical phonons. Those electrons which have energies below the phonon emission threshold can cool further only by giving up some of their energy to other electrons, to the holes, or to gain energy through the *e-e* process sufficient to emit a phonon. Thus we end up at a situation where more electrons are just below the phonon emission threshold. The slowing becomes more significant at high concentrations, as shown in Fig. 6(b),

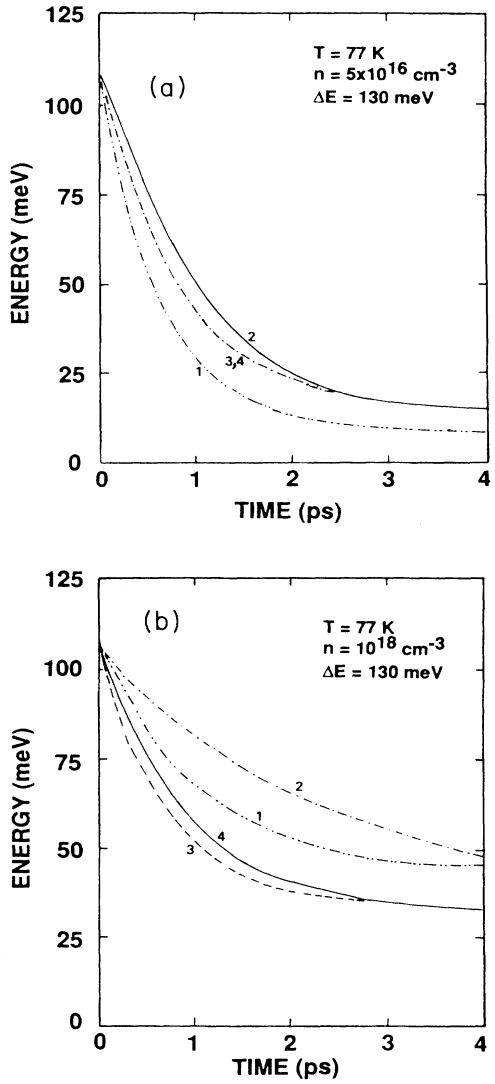

FIG. 6. The time evolution of the mean energy of the electrons for various active scattering mechanisms: curve 1, *e*-ph only; curve 2, *e*-ph and *e-e*; curve 3, *e*-ph and *e-h*; and curve 4, *e*-ph, *e-e*, and *e-h*. The material is GaAs at 77 K. (a) is for a density of 5×10^{16} cm^{-3}, while (b) is for a density of 10^{18} cm^{-3}.

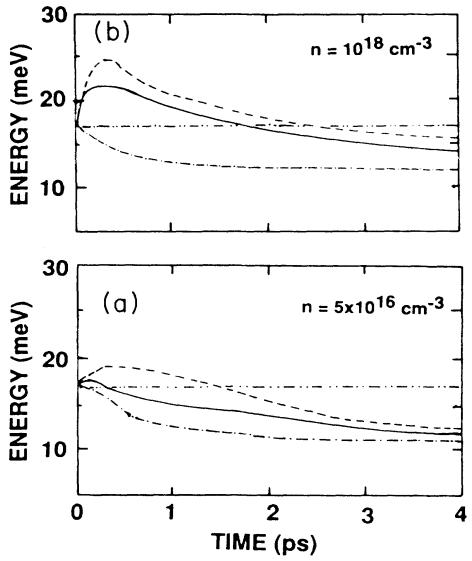

FIG. 7. The time evolution of the mean energy of the heavy holes for various active scattering mechanisms, with (a) and (b) corresponding to (a) and (b) of Fig. 6: curve 1, *h*-ph only; curve 2, *h*-ph and *h-h* only; curve 3, *h*-ph and *e-e*; and curve 4, *h*-ph, *e-h*, and *h-h*.

where the optical phonons are strongly screened and the *e-e* scattering is more frequent.

The case where only the *e*-ph and *e-h* interactions were active was then investigated to understand how these two energy-loss mechanisms contribute to the cooling of the electrons. From examining curve 3 in Fig. 7, we see that the average energy of the holes increases rapidly during the first half picosecond as a result of the energy transferred from the electrons. Notice that the increase in the average energy is larger at an excitation level of 10^{18} cm^{-3}, due to the increase in the *e-h* scattering rates. Also, the holes eventually cool down at a slower rate than when the *h-h* interaction is present, so that the holes take longer to thermalize through the *e-h* than through the *h-h* interaction. From Figs. 6(b) and 7(b), it is obvious that the electron-hole interaction enhances the cooling rate at a high carrier concentration, since the electrons channel their excess energy to the lattice through the holes. On the other hand, at low concentrations [Figs. 6(a) and 7(a)], the *e-h* scattering slows down the cooling rate by gradually shifting the electron population to lower energy states.

Finally, the more realistic situation, where all the scattering mechanisms *e-e*, *e-h*, *h-h*, *e*-ph, and *h*-ph are present, was investigated. At low concentrations, the cooling of the electrons is not affected by the added complexity, and the resulting cooling rate is identical to the situation where only the *e-h* and *h*-ph interactions were present, reflecting the fact that *e-h* scattering is efficient in moving electrons to lower states even at this low concentration, as shown by curve 4 in Fig. 6(a). At high concentrations, the *e-h* interaction is the most important factor in determining the cooling rate. The presence of the *e-e* scattering slows down the cooling rate slightly

during the first two picoseconds, during which the electron thermalization takes place through the *e-e* and *e-h* collisions [curve 4 in Fig. 6(b)]. However, for the holes, the presence of the *h-h* scattering, together with the *e-h* scattering, leads to a faster cooling rate because of the dominance of the *h-h* collisions. The cooling rates were then studied at other excitation levels, between 5×10^{16} and 10^{18} cm^{-3}, to examine the manner in which the electron-hole interaction changes with concentration. The time evolution of the mean energy of the electrons is shown in Fig. 8 for different carrier concentrations. The cooling rate slows down with increasing carrier concentrations. The holes also exhibit the same trend as shown in Fig. 9. In addition, the initial rise in the average energy is higher at higher carrier concentration. The fact that less heating is observed at 5×10^{16} cm^{-3} means that energy transfer from the electrons to the holes is small. This can be understood from the fact that the electron-hole scattering rate is proportional to the carrier concentration, so that at high concentrations the collisions occur more frequently, resulting in more energy transfer from the hot electrons to the holes, even though the energy transfer in a single collision is small. Although, at a carrier concentration of 10^{18} cm^{-3}, the *e-h* interaction leads to a faster relaxation, the cooling rate predicted by this model was found to be slower than an analytical model which includes the hot phonon effect and assumes equal electron and hole temperatures.[25] Figure 10 shows the time evolution of the average energy of the electrons and holes excited by different excitation energies. Notice that when a photon of energy 1.55 eV is used to excite the carriers, holes end up with approximately 5 meV, so that they gain energy gradually to reach equilibrium with the lattice and electrons. The energy gradient between the electrons and holes increases as the pulse energy increases, and lasts for a longer time. This will lead to an increase in the role of the *e-h* interaction which will be shown in the next section.

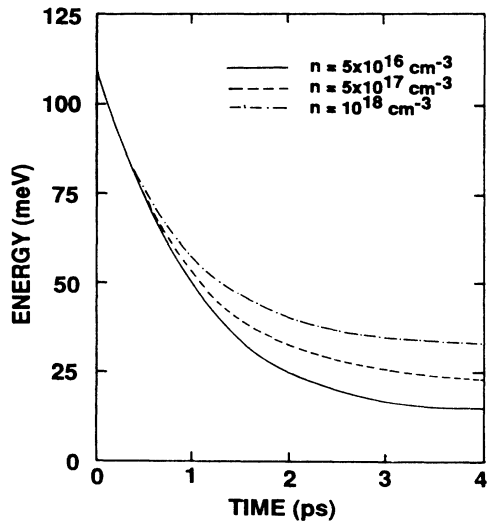

FIG. 8. The time dependence of the mean energy of the electrons excited by a 1.64-eV laser pulse, for various excited carrier densities, in GaAs at 77 K.

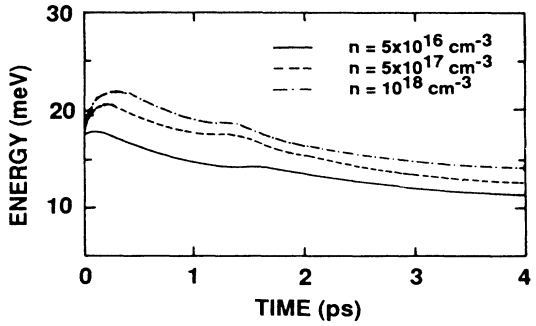

FIG. 9. The time dependence of the mean energy of the holes excited by a 1.64-eV laser pulse, for various carrier concentrations, in GaAs at 77 K.

C. The electron energy-loss rates

In order to get a measure of the rates at which the carriers cool down, the electron energy-loss rates through *e-h* and *e*-ph collisions were calculated for different excitation levels and energies. The energy transfer from the electrons to the holes is calculated from the following relationship:

$$\Delta E_{e\text{-}h}(t)=E_h(t)+\Delta E_{h\text{-ph}}(t)-E_h(0)\ , \tag{26}$$

where $\Delta E_{h\text{-ph}}(t)$ is the net energy the holes transfer to the lattice through phonon emission up to time t, and $E_h(t)$ is the average energy of the hole ensemble. From the knowledge of the amount of energy lost by the electrons via phonon emission and electron-hole interaction, we were able to obtain the energy-loss rates. In Figs. 11(a) and 11(b), the time dependence of the electron energy-loss rates through phonon emission and *e-h* interaction are shown for an *e-h* plasma excited by a 1.64-eV laser pulse at excitation levels of 5×10^{16} and 10^{18} cm^{-3}, respectively. At the lower excitation level, the electron energy-loss rate during the first picosecond through the *e*-ph interaction is five times larger than the

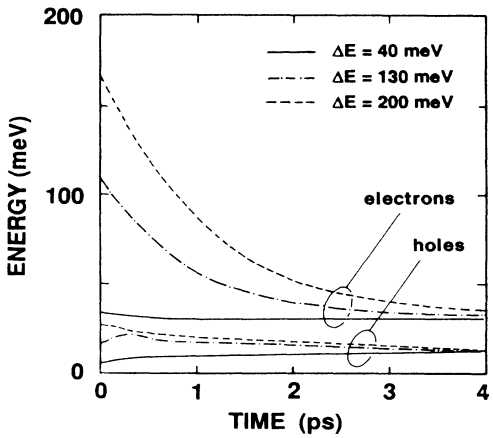

FIG. 10. The time dependence of the mean energy of the electrons and the holes, for various laser energies, at an excitation level of 10^{18} cm^{-3} at 77 K.

corresponding *e-h* interaction. On the other hand, for the higher density, the energy-loss rate through the *e-h* interaction is almost twice as large as that for the *e*-ph interaction. From these two plots, we conclude that, at low hot carrier concentrations, the cooling of electrons is controlled by the phonon emission process, while at high concentration the cooling is mainly through the transfer of energy to the cold hole plasma. This can be understood from the fact that at high carrier concentrations the *e*-ph interaction is strongly screened while the electron-hole interaction becomes stronger.

The electron energy-loss rate was further investigated at two densities intermediate between those discussed above. In Fig. 12(a), the energy-loss rate through the *e-h* interaction is plotted for all of the densities investigated. From this figure, it is obvious that the role of *e-h* interactions as an energy-loss channel becomes stronger as the carrier concentration increases. The energy-loss rates for the electrons through the *e*-ph interaction are plotted in Fig. 12(b) for the same range of concentrations. Notice that, as the carrier concentration increases above 10^{17} cm^{-3}, the energy-loss rate actually decreases for this latter mechanism due to the effect of screening. However, the magnitude of the change in the energy-loss rate through this latter interaction is smaller than that due to the *e-h* interaction. Thus it is the increased strength of the *e-h* interaction, and not the screening of the *e*-ph interaction, that is primarily responsible for determining the cooling rates of the electrons at high concentrations. From these figures, we conclude that at low concentrations the cooling of the electrons is primarily through the transfer of energy to the lattice by phonon emission, while at high concentrations the cooling is mainly through the transfer of energy to the cold hole plasma. Furthermore, the holes continue to transfer the energy gained from the electrons to the lattice through the essentially unscreened deformation-potential interaction. Figure 13 summarizes the importance of the energy-loss channels for photoexcited electrons at the lowest and highest densities discussed here. The width of the arrows is proportional to the amount of energy flow through the respective channel, and thus schematically depicts the above results.

The above results agree with the recent experimental

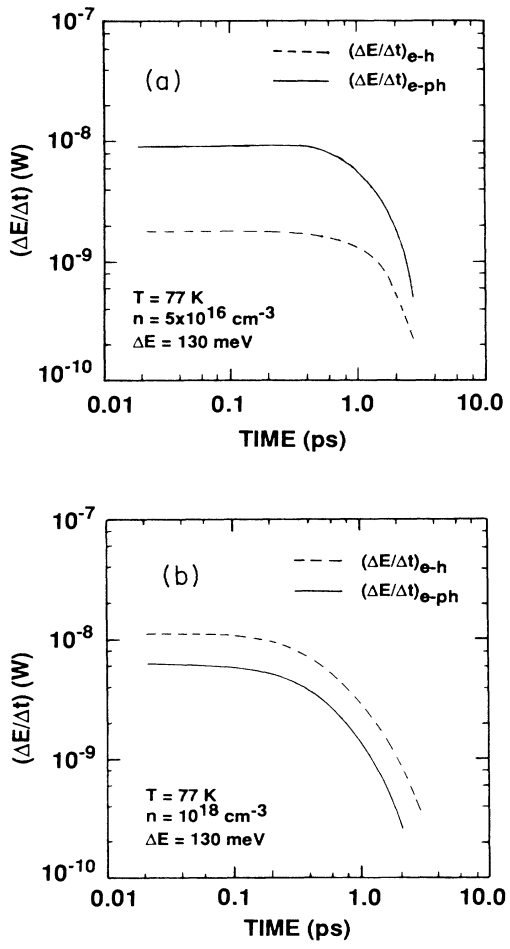

FIG. 11. The time dependence of the electron loss rates through the *e-h* and *e*-ph interactions. (a) is for a density of 5×10^{16} cm^{-3}, while (b) is for 10^{18} cm^{-3}.

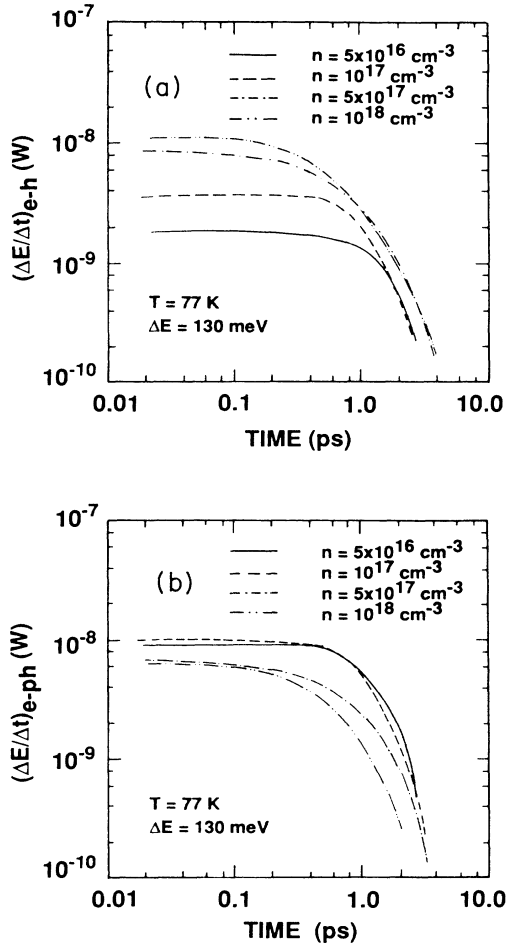

FIG. 12. The time dependence of the electron energy-loss rates, for a variety of excited-carrier densities, for (a) the *e-h* interaction, and (b) the *e*-ph interaction.

observations by Höpfel *et al.*[2] of the increase in the energy-loss rates of electrons in the presence of a cold hole plasma in multiple quantum-well structures. However, the manner in which the confined electrons in quantum wells lose energy may not be of the same order of magnitude as that for the free electron in bulk material. Additionally, the *e-h* scattering rate is mainly determined by the hole concentration, since the rate at which an electron interacts with a hole plasma is larger than the rate at which a hole interacts with an electron plasma. Therefore the role of the *e-h* interaction in the photoexcited *e-h* plasma is more or less similar to that for photoexcited minority electrons in *p*-type material.

The energy-loss rates were then examined at 1.55- and 1.71-eV photon energies at an excitation level of 10^{18} cm^{-3}. The results are shown in Fig. 14. Here, it is apparent that the *e-h* interaction becomes stronger at higher energies. From Fig. 10, it is clear that the increase in photon energies primarily increases the energy of the hot electrons, leading to higher-energy differences between the electrons and the holes. This then leads to an enhanced energy-loss rate through the *e-h* interaction.

In the presence of an external electric field, the electrons will gain energy at a higher rate than the holes due

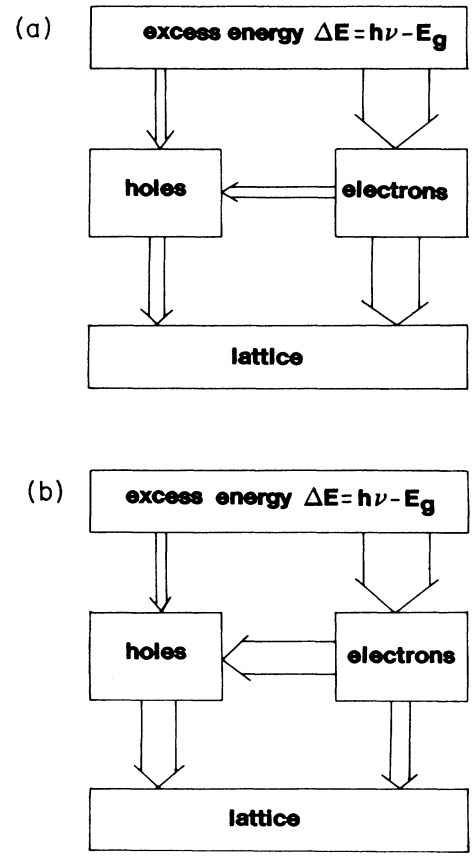

FIG. 13. The energy flow channels for energy relaxation following excitation by a 1.64-eV pulse for (a) 5×10^{16} cm^{-3} and (b) 10^{18} cm^{-3}. The width of the arrows indicates the relative size of the energy decay channel.

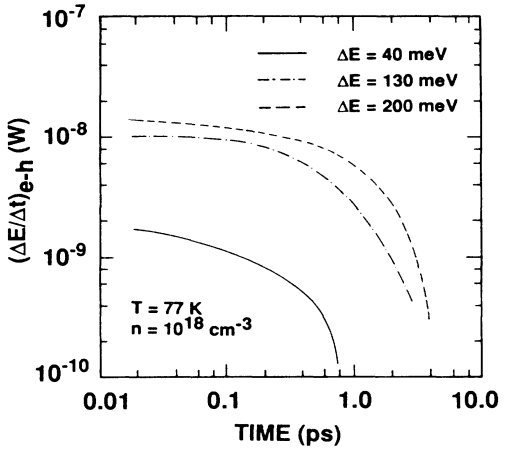

FIG. 14. The time dependence of the electron energy-loss rate through *e*-ph interactions for different initial excitation energies.

to their smaller mass.[26] However, the hotter electrons will lose more energy to the holes if there is a *p*-type background of charge. This effect will reduce the energy of the electrons and reduce their heating by the field. Moreover, since there is less electron heating, it is expected that there will be less transfer to the upper valleys.[13,27] Furthermore, since electrons and holes gain momentum in opposite directions from the field, the momentum exchange involved in the *e-h* interaction leads to reduced mobilities for the electrons at high excitation levels and *p*-type materials at high fields.[28] The same conclusions hold for quantum-well structures where the holes have higher mobilities so that the effect of momentum exchange through the *e-h* interaction is magnified. This has been suggested as the primary reason minority electrons excited in quantum wells exhibit absolute negative mobility at low fields and temperatures.[12]

D. The evolution of the carrier distributions

The presence of the *e-e* interaction manifests itself through redistribution of the energy among the electron population in such a way that there are electrons in the high-energy tails and at low energies. The same argument applies to the *h-h* interaction. Analytical models for the cooling process always assumed that this thermalization process is quite fast, so that a distribution function is rapidly established immediately following the pulse. This distribution is either Fermi-like or a Maxwellian in nature. We now want to examine how the *e-e*, *h-h*, and *e-h* interactions influence the form of the distribution function.

The energy transfer involved in an *e-h* scattering event is small on account of the large mass of the hole. In the previous section, we showed that, at low carrier concentrations, the *e*-ph interaction dominates the energy relaxation process [see Fig. 11(a)]. This is again illustrated in Fig. 15, where the distribution function displays peaks at energies localized below the laser energy at integral mul-

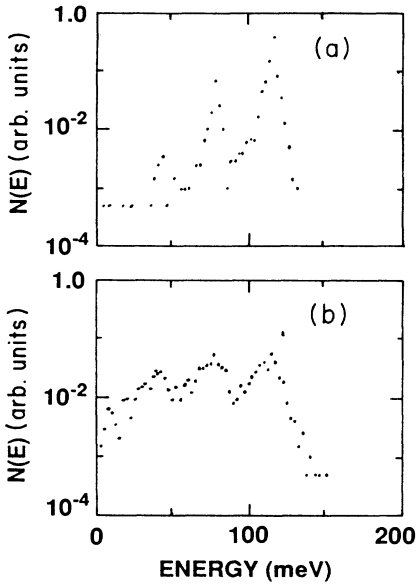

FIG. 15. The electron energy distribution after excitation by a 200-fs, 1.64-eV laser-pulse-generated density of 5×10^{16} cm^{-3}, assuming only that the *e*-ph and *e-h* interactions are active, and at times of (a) 100 fs and (b) 500 fs after start of the pulse.

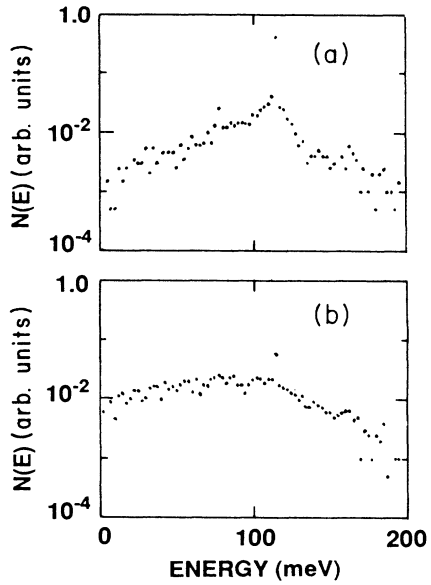

FIG. 16. The electron energy distribution function after excitation of an electron-hole plasma, with density of 10^{18} cm^{-3}, by a 1.64-eV laser pulse, with *e*-ph, *e-h*, and *e-e* interactions all present, and for times of (a) 50 fs and (b) 250 fs after the pulse.

tiples of the optical-phonon energy. In this curve, we have assumed that a 0.2-ps, 1.64-eV laser pulse was used to create the *e-h* plasma. Note that, at a time midway through the pulse, electrons have already started cascading downward by the emission of optical phonons. In addition, we see that the *e-h* and *e-e* collisions lead to broadening of the peaks that arise from phonon emission, and that there are more electrons on the lower side of the peaks, indicating a loss of energy by the electrons through the *e-h* interactions. Furthermore, even at a time of 0.5 ps after the pulse, the distribution function still exhibits marked peaks, reflecting the fact that most of the electrons cool down by emitting phonons.

At high concentrations, a different procedure results. In Fig. 16, we show the distribution function for a concentration of 10^{18} cm^{-3}. Here, the carriers thermalize faster through the *e-e* interaction and through the *e-h* interaction. The peaks that were clearly visible at lower concentrations at 0.5 ps are no longer visible, even at much shorter times. This means that the role played by the emission of optical phonons is much weaker than that of the carrier-carrier interactions. The presence of the *e-e* interaction results in more electrons being scattered to higher energy states, so that an almost smooth distribution of the carriers results at shorter times.

The manner in which the *e-e* and *e-h* interactions influence the shape of the energy distribution of electrons generated by a 1.71-eV laser pulse is demonstrated more clearly in Figs. 17–19. First, the phonon peaks are already barely visible at 0.25 ps, even in the absence of the *e-e* interaction. Furthermore, the *e-h* interaction is very dominant, and establishes a single broadened peak centered at the excitation energy (with more electrons in the lower energy states), rather than merely broadening the phonon emission peaks. The introduction of the *e-e* interaction thoroughly washes out the individual peaks, weakens the central peak, and pushes more electrons both to lower and higher energies. This results in a very smooth distribution function at 0.5 ps, as shown in Fig. 18(b). From these plots, and also from

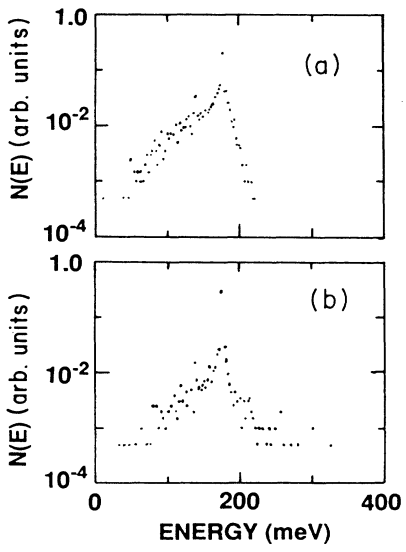

FIG. 17. The electron energy distribution after excitation by a 1.71-eV laser pulse, and a density of 10^{18} cm^{-3}. (a) is the case where only *e*-ph and *e-h* interactions are included, and the time is 250 fs, while (b) is for *e*-ph, *e-e*, and *e-h* scattering and a time of only 100 fs.

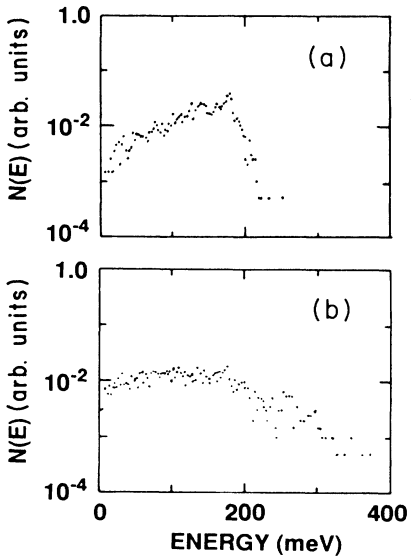

FIG. 18. The electron energy distribution function after excitation by a 1.71-eV laser pulse, and a concentration of 10^{18} cm^{-3}, 500 fs after the pulse. (a) is for *e*-ph and *e-h* interactions only, while (b) includes the *e-e* interaction as well.

the distribution function in momentum space, we have found that the *e-e* interaction determines the shape of the distribution function. However, this distribution may not have a standard (Maxwellian or Fermi-Dirac) form at times less than 0.5 ps, even though a smooth distribution may be found at earlier times. The large spread in the energy distribution persists even at times of 1.0 ps after the pulse, as shown in Fig. 19(b). The high-energy tails disappear from the energy and momentum distributions, and a "standard" form is obtained, only after 2.0 ps. At these longer times, no distinction can be made from the shape of the distribution obtained ignoring *e-e* scattering and that shape obtained by including all scattering processes. Thus the final shape is determined largely by the *e-h* process.

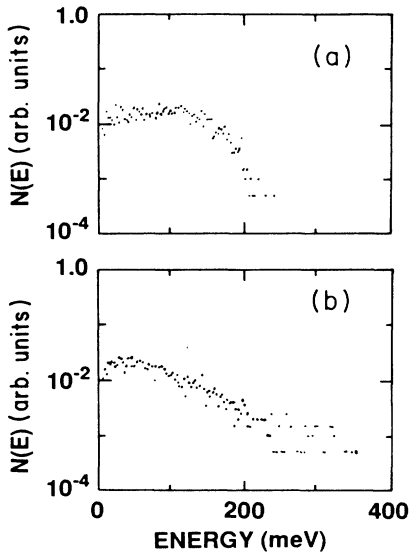

FIG. 19. The electron energy distribution after excitation by a 1.71-eV laser pulse to a concentration of 10^{18} cm^{-3}, 1 ps after the initial pulse. (a) includes only the *e*-ph and *e-h* interactions, while (b) includes the *e-e* interactions as well.

V. CONCLUSIONS

A detailed ensemble Monte Carlo model for the analysis of the ultrafast relaxation of photoexcited carriers in GaAs has been presented. The expressions for the scattering rates for the *e-h*, screened *e*-ph, and *h*-ph interactions were developed. The scattering rates for *h-h* interactions are quite large in comparison to the *e-e* rates, due to the difference in the final-state densities. The screening of the *e*-ph interaction leads to a significant reduction in the scattering rates, especially at high carrier concentrations and low temperatures. The screening is included in a self-consistent, but long-wavelength, approximation to take advantage of the built-in, time-evolving distribution function inherent in the EMC approach. The model does not make any assumptions about the form of the distribution functions or about the individual or average energies of the electrons and holes.

For an *e-h* plasma generated by a 1.55-eV laser pulse, with a generated density between 5×10^{16} and 10^{18} cm^{-3}, we have shown that the *e-h* interactions slow the cooling rate of the photoexcited electrons at low excitation levels by shifting the electron population to energies below the phonon emission threshold. The *e-e* interaction results in the same behavior. On the other hand, at high concentrations, the *e-h* interaction enhances the cooling rates by transferring the electron energy to the holes. These results suggest that at low densities, the energy flow from the electrons to the lattice is primarily through the *e*-ph interaction, while at high concentrations it is primarily through the *e-h* interaction and then through the *h*-ph interaction. This latter proceeds primarily through the unscreened TO deformation-potential interaction.

The holes themselves have a modified behavior in the presence of the *c-c* interactions. The *h-h* interactions enhance the cooling of the holes by shifting a fraction of the holes to states above the threshold for the emission of phonons. Normally, the photoexcited holes sit too low in energy for this process.

The presence of the *e-e* and *h-h* interactions is necessary to achieve the rapid randomization of energy and momentum in the respective distributions. At higher laser energies, the loss rate of the electrons through the *e-h* interaction is further increased, a result that is also achieved by increasing values of the electric field.

Although the results predicted by this model give qualitative agreement with the experimental results obtained by others, a more general model should include the possibility of nonequilibrium phonons and inelastic

acoustic scattering, as well as the coupled modes of the plasmons and phonons. Furthermore, the complex structure of the valence band and the overlap function behavior of the *e-h* interaction should be included to try to understand the orientation dependence of the momentum and energy relaxation processes that has been observed.[29] Investigations of these processes are currently underway.

ACKNOWLEDGMENTS

The authors express their appreciation for many stimulating discussions with Dr. P. Lugli and Dr. L. Reggiani of the University of Modena, Dr. V. Ravaioli and Dr. W. Pötz of the University of Illinois, and Dr. O. Sankey of Arizona State University. This work was supported by the U.S. Office of Naval Research.

*Present address: Scientific Research Associates, P.O. Box 498, Glastonbury, CN 06033.

[1]J. Shah, A. Pinczuk, A. C. Gossard, and W. Wiegmann, Phys. Rev. Lett. **54**, 2045 (1985).

[2]R. A. Höpfel, J. Shah, and A. C. Gossard, Phys. Rev. Lett. **56**, 765 (1986).

[3]J. A. Kash, J. C. Tsang, and J. Hvam, Phys. Rev. Lett. **54**, 2151 (1985).

[4]C. L. Collins and Y. Yu, Solid State Commun. **51**, 123 (1984).

[5]C. V. Shank, R. L. Fork, B. I. Greene, F. K. Reinhart, and R. A. Logan, Appl. Phys. Lett. **38**, 104 (1981).

[6]A. C. S. Algarte, Phys. Rev. B **32**, 2388 (1985).

[7]W. Pötz and P. Kocevar, Phys. Rev. B **28**, 7040 (1980).

[8]R. Luzzi and A. R. Vasconcellos, in *Semiconductors Probed by Ultrafast Laser Spectroscopy,* edited by R. R. Alfano (Academic, Orlando, 1984), Vol. 1, p. 135.

[9]M. Asche and O. G. Sarbei, Phys. Status Solidi B **126**, 607 (1984).

[10]H. Ehrenreich, J. Phys. Chem. Solids **9**, 129 (1959).

[11]N. Takenaka, M. Inoue, and Y. Inishi, J. Phys. Soc. Jpn. **47**, 861 (1979).

[12]R. A. Höpfel, J. Shah, P. A. Wolf, and A. C. Gossard, Phys. Rev. Lett. **56**, 2736 (1986).

[13]R. J. Degani, R. F. Leheny, R. E. Nahory, and J. P. Heritage, Appl. Phys. Lett. **39**, 569 (1981).

[14]J. Zimmerman, P. Lugli, and D. K. Ferry, Solid-State Electron. **26**, 233 (1983).

[15]U. Ravaioli, Ph.D. thesis, Arizona State University, Tempe, AZ, 1986.

[16]K. Brennan and K. Hess, Phys. Rev. B **29**, 5581 (1984).

[17]O. Madelung, in *Physics of Group IV Elements and III-V Compounds,* Vol. 17a of *Landolt-Börnstein,* edited by K. H. Hellwege (Springer-Verlag, Berlin, 1981).

[18]J. D. Wiley and M. DiDomenico, Phys. Rev. B **2**, 427 (1970).

[19]d. Kranzer, Phys. Status Solidi A **26**, 11 (1974).

[20]D. K. Ferry, Phys. Rev. B **18**, 7033 (1978).

[21]J. Collet, A. Cornet, M. Pugnet, and T. Amand, Solid State Commun. **42**, 883 (1982).

[22]P. Lugli and D. K. Ferry, IEEE Trans. Electron Devices ED-**32**, 2431 (1985).

[23]P. Lugli and D. K. Ferry, Physica **117B**, 251 (1983).

[24]C. Jacoboni and L. Reggiani, Rev. Mod. Phys. **55**, 645 (1983).

[25]M. A. Osman, U. Ravaioli, R. Joshi, W. Pötz, and D. K. Ferry, in *Proceedings of the 18th International Conference on the Physics of Semiconductors,* edited by O. Engstrom (World Scientific, Singapore, 1987), p. 1311.

[26]M. A. Osman, U. Ravaioli, and D. K. Ferry, in *High Speed Electronics,* edited by B. Kallback and H. Beneking (Springer-Verlag, Heidelberg, 1986).

[27]M. A. Osman and D. K. Ferry, J. Appl. Phys. **61**, 5330 (1987).

[28]D. D. Tang. F. F. Fang, M. Scheuermann, and T. C. Chen, Appl. Phys. Lett. **49**, 1540 (1986).

[29]J. L. Oudar, A. Migus, D. Hulin, A. Grillon, J. Etchepare, and A. Antonetti, Phys. Rev. Lett. **53**, 384 (1984).